



HAL
open science

On Mars's Atmospheric Sputtering After MAVEN's First Martian Year of Measurements

François Leblanc, Antoine Martinez, Jean-Yves Chaufray, Ronan Modolo, T. Hara, J. Luhmann, R. Lillis, S. Curry, J. Mcfadden, J. Halekas, et al.

► **To cite this version:**

François Leblanc, Antoine Martinez, Jean-Yves Chaufray, Ronan Modolo, T. Hara, et al.. On Mars's Atmospheric Sputtering After MAVEN's First Martian Year of Measurements. *Geophysical Research Letters*, 2018, 45, pp.4685-4691. 10.1002/2018GL077199 . insu-03737439

HAL Id: insu-03737439

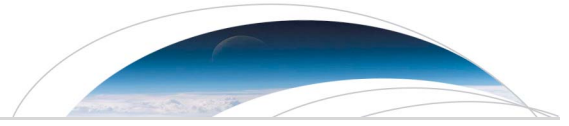
<https://insu.hal.science/insu-03737439>

Submitted on 25 Jul 2022

HAL is a multi-disciplinary open access archive for the deposit and dissemination of scientific research documents, whether they are published or not. The documents may come from teaching and research institutions in France or abroad, or from public or private research centers.

L'archive ouverte pluridisciplinaire **HAL**, est destinée au dépôt et à la diffusion de documents scientifiques de niveau recherche, publiés ou non, émanant des établissements d'enseignement et de recherche français ou étrangers, des laboratoires publics ou privés.

Copyright



RESEARCH LETTER

10.1002/2018GL077199

Key Points:

- Reconstruction of the average precipitating flux into Mars's atmosphere based on MAVEN's first 2 years of measurements is presented
- Reconstruction of the sputtering contribution to Mars's exosphere using MAVEN-measured precipitating flux is presented
- A comparison with other sources of exosphere allows us to suggest where sputtering signatures in the exosphere might be detectable

Correspondence to:

F. Leblanc,
francois.leblanc@latmos.ipsl.fr

Citation:

Leblanc, F., Martinez, A., Chaufray, J. Y., Modolo, R., Hara, T., Luhmann, J., et al (2018). On Mars's atmospheric sputtering after MAVEN's first Martian year of measurements. *Geophysical Research Letters*, 45, 4685–4691. <https://doi.org/10.1002/2018GL077199>


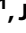






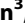


Received 20 JAN 2018

Accepted 5 MAR 2018

Accepted article online 23 MAR 2018

Published online 18 MAY 2018

On Mars's Atmospheric Sputtering After MAVEN's First Martian Year of Measurements

F. Leblanc⁶ , A. Martinez¹ , J. Y. Chaufray¹ , R. Modolo² , T. Hara³ , J. Luhmann³ , R. Lillis³ , S. Curry³ , J. McFadden³ , J. Halekas⁴ , and B. Jakosky⁵ 

¹LATMOS/IPSL, CNRS, Sorbonne Université, UVSQ, Paris, France, ²LATMOS/IPSL, UVSQ Université Paris-Saclay, UPMC Université Paris 06, CNRS, Guyancourt, France, ³Space Sciences Laboratory, University of California, Berkeley, CA, USA, ⁴Department of Physics and Astronomy, University of Iowa, Iowa City, IA, USA, ⁵Laboratory for Atmospheric and Space Physics, University of Colorado Boulder, Boulder, CO, USA, ⁶NASA Goddard Space Flight Center, Greenbelt, MD, USA

Abstract Mars likely lost a significant part of its atmosphere to space during its history. The sputtering of the atmosphere, by precipitating planetary heavy pickup ions accelerated by the solar wind, is one of the processes that could have significantly contributed to this atmospheric escape, in particular since the cessation of its global magnetic field, 4.0–4.1 Gyr ago. We present a 2 year baseline analysis of Mars Atmosphere and Volatile Evolution (MAVEN) observations of the precipitating flux. We use this measurement to model the expected escape rate and exospheric structure induced by this precipitation. We conclude that sputtering signatures in the dayside exosphere will be difficult to identify by MAVEN, and the induced atmospheric escape of O atoms remains orders of magnitude smaller than the expected rate induced by dissociative recombination of O₂⁺ in Mars's ionosphere. On the contrary, deep in the nightside, Mars's sputtering might be the main source of the nonthermal part of the exospheric density profiles of species with mass larger or equal to Ar.

Plain Language Summary After 2 years of Mars Atmosphere and Volatile Evolution measurements, it is possible to reconstruct the average precipitating heavy ion flux into Mars's atmosphere. These ions can lead to the sputtering of Mars's atmosphere, a process which might have eroded a significant part of Mars's atmosphere 4 Gyr ago. Today, it is much more difficult to identify a clear signature of this process. However, we here show that such signature might be found deep in the night according to models.

1. Introduction

The main objective of Mars Atmosphere and Volatile Evolution (MAVEN) mission is to characterize Mars's present atmospheric escape, its main drivers, and to reconstruct its past evolution (Jakosky et al., 2015). To achieve these goals, MAVEN's strategy consists of identifying signatures of the various channels of atmospheric escape and estimating their importance and dependence with respect to solar wind conditions (Lillis et al., 2015). Among these channels, sputtering of the Martian atmosphere by precipitating heavy ions has been identified as one of these potential channels (Luhmann & Kozyra, 1991). The first evidence of heavy ion precipitation for nominal solar wind conditions has been reported by Leblanc et al. (2015), highlighting that sputtering should clearly occur at Mars. Hara et al. (2017), analyzing the first 1.5 years of MAVEN measurements, showed that this precipitation is organized with respect to the orientation of the solar wind convection electric field and is dependent on the upstream solar wind conditions. Hara et al. (2018) also highlighted the role of the crustal magnetic field in the local increase of this precipitating flux.

However, no clear signature of the consequences of these precipitating heavy ions on the structure of the Martian atmosphere could be identified, as an example, in the oxygen atomic exosphere or in the thermosphere (Fang et al., 2013; Leblanc et al., 2017). Bhardwaj et al. (2017) suggested that the part of the Ar density profiles measured by Neutral Gas and Ion Mass Spectrometer and Mars Exospheric Neutral Composition Analyser/Mars Orbiter Mission above 250 km in altitude could be significantly changed by such precipitation, a conclusion we will address here by modeling the expected density profiles associated with the typical range of ion precipitation measured by MAVEN.

In this paper, we present the first estimate of sputtered escape induced by the precipitating energy flux measured by MAVEN. We also determine how the exosphere could be shaped by the sputtered atmospheric

ejecta by using the Exospheric Global Model (EGM; Leblanc et al., 2017) developed to describe Mars's exosphere at any Martian season and solar activity. We compare the spatial structure of the exosphere as produced by sputtering with the one produced by dissociative recombination of the dominant ion O_2^+ in Mars's ionosphere and estimate the contribution of sputtering to Mars's atmospheric erosion. In section 2, we present MAVEN measurements of precipitating ions based on one Martian year of measurements. In section 3, the simulated signatures induced by these precipitating ions are described using EGM, and in section 4 we conclude.

2. Measurements

In order to reconstruct the flux of precipitating ion measured by MAVEN, we used the same approach as in Leblanc et al. (2015) and Leblanc et al. (2017), that is, we used all available measurements of the ion mass and energy distributions realized between 200 and 350 km in altitude by the Solar Wind Ion Analyzer (SWIA; Halekas et al., 2015) and by the Supra-Thermal And Thermal Ion Composition (STATIC; McFadden et al., 2015). STATIC is an energy, mass, and angular ion spectrometer operating in the range of 0.1 eV/q to 30 keV/q (energy resolution between 11 and 16%), with a field of view (FOV) of $360^\circ \times 90^\circ$ (with 22.5° resolution) and a mass range from 1 to 70 amu. STATIC has a mass resolution large enough to separate the main ion species: O_2^+ , CO_2^+ , and O^+ . For this study, we used the d0 product of STATIC measurements with 128 to 512 s time resolution corresponding to 32 bins in energy, 8 bins in mass, and 16 bins along the polar direction. STATIC is mounted on the Articulated Payload Platform, which points STATIC's field of view into the RAM direction at periapsis. SWIA is an energy and angular ion spectrometer covering an energy range 25 eV/q to 25 keV/q (with 48 logarithmically spaced energy steps) and a broad $360^\circ \times 90^\circ$ FOV. SWIA is positioned on the spacecraft (S/C) deck in order to observe the direction of the solar wind most of the time and also to observe the nadir direction around periapsis. In this paper, we used the coarse survey (cs) product of SWIA with an angular coverage of $360^\circ \times 90^\circ$, an angular resolution of $22.5^\circ \times 22.5^\circ$, and a temporal resolution of 4 s.

In order to reconstruct the energy distribution of the precipitating flux, we selected all portions of MAVEN orbit between 200 and 350 km in altitude. We then used data from anodes whose FOV was within the 75° cone angle centered along the zenith direction (Leblanc et al., 2015). We then selected the measurements during which the average FOV of each instrument during the path between 200 and 350 km covered more than 70% of this 75° cone angle. This criterion restricts us to a relatively small fraction of the observations performed by MAVEN during this Martian year (between 2 December 2014 and 31 October 2016), namely

1. for SWIA, 785 paths on the nightside and 839 paths on the dayside, from the 7,244 available measurements,
2. for STATIC d0, 124 paths on the nightside and 259 paths on the dayside, from the 7,268 available measurements.

The global coverage of these set of measurements still allows us to obtain uniform coverage of the Mars-Sun Orbital (MSO) latitude-longitude frame. Figure 1a displays the average precipitating flux measured by MAVEN SWIA and STATIC during the first 2 years of MAVEN operations (between 2 December 2014, $L_s = 243^\circ$, and 31 October 2016, $L_s = 247^\circ$).

As shown in Figure 1a, there is globally a good agreement (within the dispersion of the measurements indicated by the vertical bars) between the averaged measured flux by SWIA (red line) and STATIC (blue and green lines), despite the fact that SWIA field of view allows a better coverage of the cone angle pointing toward the zenith than STATIC. The comparison suggests that, when averaging the dayside and nightside, there is an equivalent number of O^+ (green line) and H^+ (blue line) precipitating toward the atmosphere. In Figure 1b we plotted the reconstructed precipitating fluxes for the measurements done by MAVEN on the dayside (solid line) and on the nightside (dashed line). There is an asymmetry between dayside and nightside, with a flux approximately 2 times larger on the dayside with respect to the nightside above 100 eV (red solid and dashed lines). Comparing STATIC flux distribution for masses between 12 and 21 amu (green dashed lines) and SWIA flux (all masses, dashed red line), the precipitating flux on the nightside appears to be dominated below 1,000 eV by ions with masses other than the O^+ mass. Such results were also suggested by Hara et al. (2018).

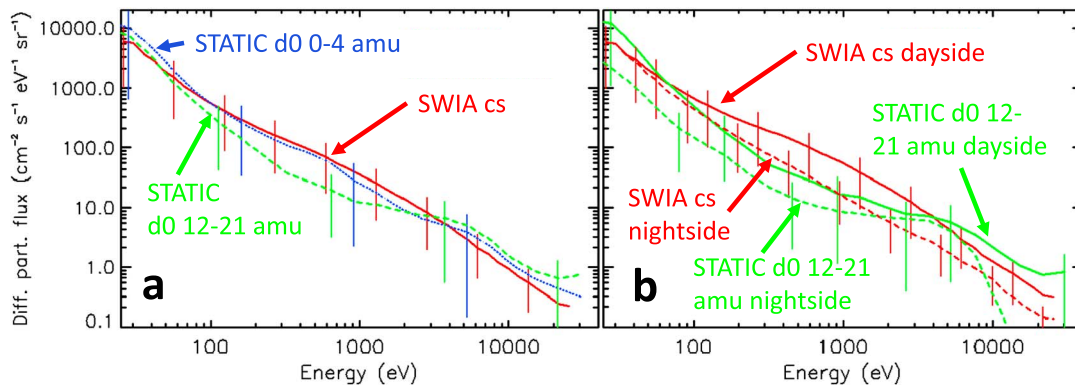


Figure 1. Differential particle flux of the precipitating ion as measured by Mars Atmosphere and Volatile Evolution between 200 and 350 km in altitude during the 2 December 2014 to 31 October 2016 period. (a) Average flux, solid red line: Solar Wind Ion Analyzer (SWIA) cs; dashed green line: Supra-Thermal And Thermal Ion Composition (STATIC) d0 12–21 amu mass range; dotted blue line: STATIC d0 0–4 amu range. (b) Dayside average flux measured by SWIA (solid red line) and STATIC (d0 product for masses between 12 and 21 amu, in solid green line) and nightside average flux measured by SWIA (dashed red line) and STATIC (d0 product for masses between 12 and 21 amu, in dashed green line). Vertical bars represent the one sigma dispersion of the measurements.

3. Application to EGM

Using the precipitating flux measured by MAVEN for the dayside and nightside (STATIC d0 product measured fluxes displayed with green lines in Figure 1b), we simulated the fate of precipitating pickup O^+ ions into Mars’s atmosphere using EGM (Leblanc et al., 2017) coupled to Laboratoire de Météorologie Dynamique-Global Circulation Model (LMD-GCM), including the ion dynamics (Chaufray et al., 2014) in order to calculate the induced exosphere and atmospheric escape by the precipitating ion. EGM is a multispecies parallelized 3-D model describing, for any season and solar conditions, how energetic O^+ ions collisionally interact with Mars’s upper atmosphere (simulated by LMD-GCM for the main neutral atmospheric species CO_2 , CO , Ar , O , and N_2). To describe the collision, we used at low energy the universal collision scheme of Lewkow and Kharhenko (2014) and at high-energy molecular dynamics scheme (Leblanc & Johnson, 2002) in order to take into account the possibility of molecular dissociation (Leblanc et al., 2017). Here the LMD-GCM model provided a description of the state of the upper atmosphere, that is, the thermosphere and ionosphere, at $L_s = 0^\circ, 90^\circ, 180^\circ,$ and 270° for solar mean conditions, representative of the period between 2 December 2014 and 24 October 2016.

In the following, we use EGM to describe the effect of these precipitating particles on Mars’s atmosphere focusing on the induced exosphere and atmospheric escape. In order to compare these effects to other atmospheric sources of the exosphere or atmospheric escape, EGM is also used to describe the contribution of dissociative recombination of O_2^+ to the exosphere and atmospheric escape, the 3-D spatial distribution of the O_2^+ being provided by LMD-GCM (Chaufray et al., 2014). We also include a description of the exospheric thermal component, that is, the thermal extension of any neutral atmosphere above the exobase (Yagi et al., 2012). In Figure 2, we show profiles for the three main species of Mars’s atmosphere, O , CO_2 , and N_2 as well as for Ar which is particularly interesting in the context of MAVEN observations and of the sputtering. Indeed, Jakosky et al. (2017) suggested that the Ar isotopic fractionation measured by MAVEN might be interpreted as a signature of Mars’s past atmospheric escape due to sputtering.

As shown in Figure 2, there is a clear transition between an exosphere dominated by the thermal component (characterized by small-scale height) and by the nonthermal component (characterized by large-scale height and produced by dissociative recombination and sputtering). This transition depends on species and local time. As an example, it occurs around 600 km for the atomic oxygen exospheric component on the dayside (Figures 2a–2c, 2e, and 2f) and around 500 km in altitude on the nightside (Figure 2d), the thermosphere being colder on the nightside. For N_2 , such a transition occurs slightly above 400 km, whereas it is around 350 km for CO_2 and Ar . There is a clear difference at low altitudes between CO_2 and Ar at the dawn equator due to the thermal component of the exosphere derived from the thermosphere modeled by LMD-GCM. The exospheric density profiles of CO_2 and Ar are close to each other on the nightside, at dawn, and at the poles. They diverge gradually on the dayside with increasing local time, the CO_2 exospheric density being up to 8 times larger at the dusk equator than the Ar density at 1,500 km in altitude. This divergence is due to a change

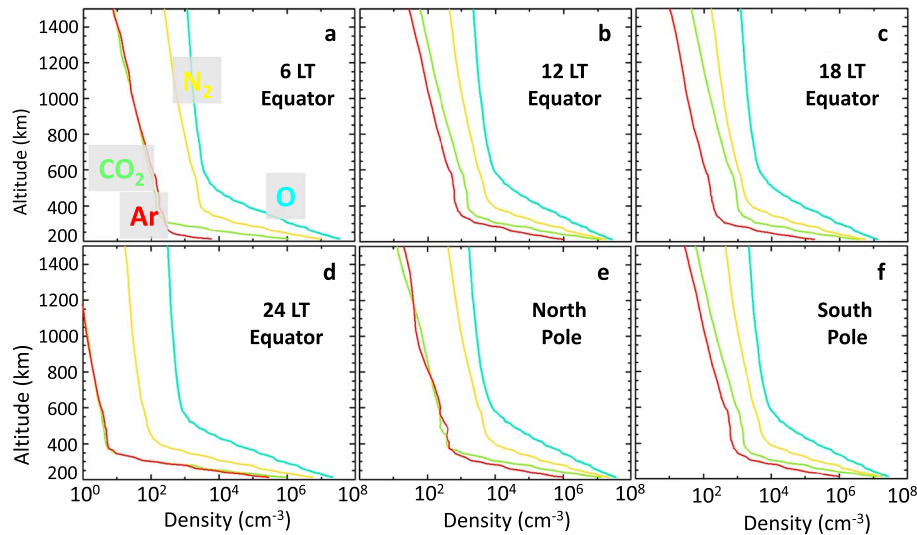


Figure 2. Atmospheric profile (O, CO₂, N₂, and Ar) at 6 LT equator (a), at 12 LT equator (b), 18 LT (c) equator, 24 LT (d) equator, North pole (e), and South pole (f) from 200 to 1,500 km in altitude (Ls = 180°, autumn equinox). Blue line: O density, yellow line: N₂ density, green line: CO₂ density, and red line: Ar density.

of the mixing ratio of Ar and CO₂ with increasing local time. These results, displayed for Ls = 180° in Figure 2, are essentially similar at the three other Ls considered in this work, Ls = 0°, 90°, and 270°.

Because the profiles in Figure 2 are built from three sources: a component from the thermal expansion of the atmosphere, a component induced by dissociative recombination of O₂⁺ and one by sputtering, we separate these contributions in Figure 3 for two of the profiles displayed in Figure 2. As illustrated in Figure 3 for O and Ar, the dissociative recombination of O₂⁺ appears to be the main source of the exosphere for all species ejected into the exosphere on the dayside above 600 km in altitude (by 2 orders of magnitude with respect to the density induced by sputtering) and also for O, C, CO, N, and N₂ on the nightside. In the case of Ar and CO₂ on the nightside, sputtering above 300 km in altitude is the main source of the exosphere. Dissociative recombination of O₂⁺ is indeed not only a source of atomic oxygen escape and of a nonthermal oxygen component in the exosphere. The dissociative recombination of O₂⁺ produces nonthermal oxygen atoms with energies up to 3.5 eV, which can collide with all thermospheric species. These collisions can therefore

produce recoiled particles with energy significantly larger than the local thermal energy, recoiled particles that can reach high altitudes and populate the exosphere. Above a given altitude, these nonthermal particles get much more than the thermal exospheric particles leading to the two slopes density profile shown in Figure 3. Figure 3 shows that even for a species like Ar, the main origin of its density profile in the exosphere is not sputtering, as interpreted by Bhardwaj et al. (2017), but collisions with the nonthermal oxygen atoms produced by dissociative recombination. However, this conclusion is valid only on the dayside and on the nightside for some species. Indeed, species as O, C, N, CO, and N₂ when ejected from the dayside into the exosphere can ballistically populate the whole nightside exosphere. But heavier species as CO₂ or Ar do not get enough energy on the dayside to reach the deep nightside. As a consequence, near midnight, the main source of exospheric CO₂ and Ar is sputtering, dissociative recombination being significantly reduced due to the very low O₂⁺ density at such local time (few orders smaller than on the dayside; Chaufray et al., 2014).

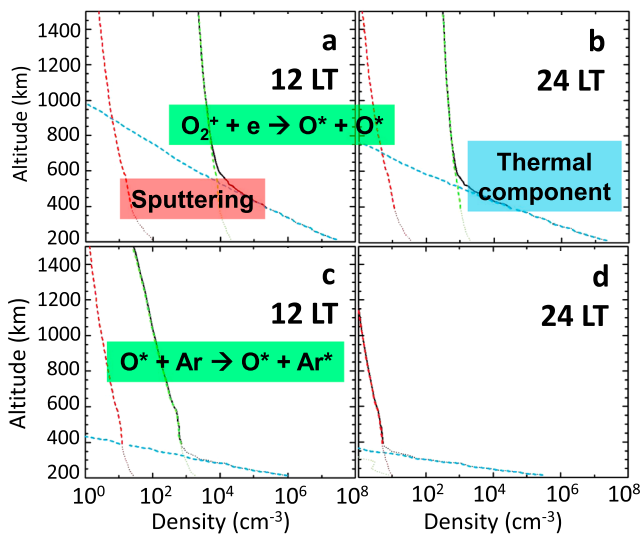


Figure 3. Atmospheric profile of O (a and b) and Ar (c and d) species at 12 LT (a to c) and 24 LT (b to d) at equator (b to d) from 200 to 1,500 km in altitude at Ls = 180°. Sputtering (red dashed line), thermal (blue dashed line), and RD O₂⁺ components (green dashed line) and total (dark dashed line).

In Figure 4, we displayed the evolution of the escape rate over one Martian year for both nonthermal processes considered in this work, the dissociative recombination of O₂⁺ (panel a) and the sputtering

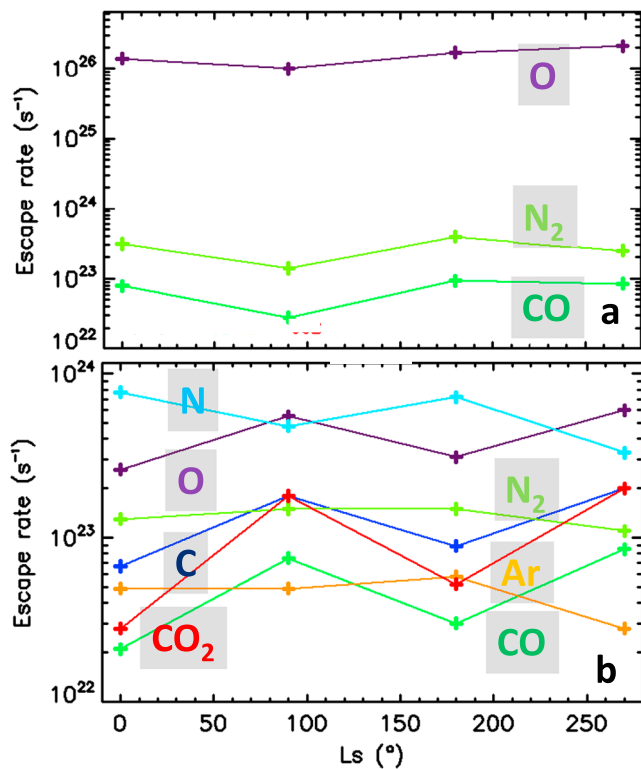


Figure 4. Escape rates of the main heavy Martian species at four Martian seasons ($L_s = 0^\circ, 90^\circ, 180^\circ,$ and 270°) induced by the dissociate recombination of O_2^+ (a) or by sputtering (b).

(panel b). It might be surprising to find a nonzero escape rate of N_2 and CO induced by the dissociative recombination of O_2^+ , the escape energy of N_2 and CO being very close to the maximum energy released by the dissociative recombination of O_2^+ . Actually, we found that around 0.01% of the test particles of N_2 or CO could reach 3 Mars radii (RM), which is the upper limit of our simulation domain where we considered particles as lost because of having a large probability of ionization before reimpacting Mars. Indeed, only 2.3 eV are needed for a N_2 or CO molecule to reach 3 RM starting from the ionosphere, so that there is a small nonzero probability for a nonthermal O atom to provide such an energy to N_2 or CO. Averaging the values displayed in Figure 4 along one Martian year, the escape rates induced by dissociative recombination of O_2^+ is 1.5×10^{26} O/s, 2.7×10^{23} N_2 /s, and 7.1×10^{22} CO/s. Supposing that the precipitating flux displayed in Figure 1 is representative of the average precipitation over a Martian year and that EGM provides a realistic description of sputtering, this process should then have induced between December 2014 and October 2016 an escape of 4×10^{23} O/s, 1.3×10^{23} C/s, 5.4×10^{23} N/s, 4.7×10^{23} CO/s, 1.2×10^{23} N_2 /s, 4.2×10^{22} Ar/s, and 9.6×10^{22} CO₂/s. Wang et al. (2015) calculated a theoretical analytical relation relating precipitating flux and induced atmospheric escape. Based on their approach, we would have found an escape rate of 1×10^{24} O/s (Leblanc et al., 2015), which is consistent with the smaller escape rate calculated in this paper, since a large part of the energy of the incident particle went into N and N_2 atmospheric loss rather than O, N, and N_2 and was not considered in the Wang et al. (2015) simulation. We did not include other photochemical reactions that should also contribute to atmospheric escape and to the exosphere, namely, the dissociative recombination of N_2^+ (Fox & Hać, 1997), the photodissociation of CO and dissociative recombination of CO^+ (Fox & Bakalian, 2001) and the dissociative recombination of CO_2^+ (Fox, 2004; Gröller et al., 2014). All these reactions are indeed usually considered as marginally contributing to the atmospheric escape compared to O_2^+ dissociative recombination.

Lee et al. (2015) published estimates of the escape rate for solar mean conditions at the same four seasons as displayed in Figure 4 and found 2.18, 1.94, 2.68, and 3.46×10^{25} O/s at $L_s = 0^\circ, 90^\circ, 180^\circ,$ and 270° , respectively. This is roughly 6 times smaller than our present estimate. It follows the same dependency with L_s , with a maximum at $L_s = 270^\circ$ (perihelion) and a minimum at $L_s = 90^\circ$ (aphelion). We discussed this issue in Leblanc et al. (2017) showing that at least a factor 3 difference can be retrieved by using the same cross sections. We also performed detailed comparison between our two models and with the Fox et al. (2014) calculation of escape probability and did not find significant differences between our two models that might explain the remaining factor 2 difference between them.

The composition of the atmospheric escape induced by sputtering (Figure 4b) is thought to be stoichiometrically related to the composition of the part of the atmosphere where energy deposition of the incident ions occurs (Johnson et al., 2000). Whereas a 1,000 eV particle deposits most of its energy around 140 km in altitude, the escape probability for atmospheric particle with few eVs starts to be significant above 150 km in altitude for solar mean conditions. Typically, averaged over the whole atmosphere, the escape probability of a particle with few eV starts to be larger than 0.1 above 160 km at $L_s = 0^\circ$ and $L_s = 180^\circ$, above 150 km at $L_s = 90^\circ$ (aphelion), and 170 km at $L_s = 270^\circ$ (perihelion). Considering the escape rates of Ar and N_2 summed with half of the escape rate of the N atoms (because these atoms come from the dissociation of the N_2 molecules impacted by the precipitating particle and by their recoils), we found an excellent agreement (within 10%) between the ratio of these escape rates and the ratio of the average abundances of Ar and N_2 at these altitudes for the four seasons (Chaufray et al., 2014). In other words, the composition of the atmospheric escape induced by sputtering is close to the composition of the atmosphere at an altitude where the probability of escape of particles with a few eV starts to be larger than 0.1.

4. Conclusion

Using the precipitating flux of heavy ions measured during the first Martian year of MAVEN's science mission, we simulate the expected signatures induced by the sputtering of Mars's upper atmosphere using EGM (Leblanc et al., 2017). Both induced exospheric densities and atmospheric escape are negligible when compared to the equivalent contributions caused by the dissociative recombination of the main ion, O_2^+ , in Mars's ionosphere. The only place, where the exospheric density increase caused by sputtering might be observable, is deep in the nightside for the heaviest atmospheric species Ar and CO_2 . However, one of the challenges to identify such signature in MAVEN data is to distinguish an exospheric profile induced by dissociative recombination and sputtering from one induced by thermospheric waves (England et al., 2017).

These results are valid for average conditions and do not preclude the possibility of identifying sputtering signatures when the precipitating flux increases significantly with respect to the average flux shown in this paper (Leblanc et al., 2017). As an example, Hara et al. (2018) and Hara et al. (2017) have shown that large variation of the precipitating flux can be expected in correlation with the solar wind pressure, the orientation of the electric field of convection, and with the presence of crustal magnetic fields.

Extrapolating the present calculation to past solar conditions remains a very uncertain exercise without constraints on the dependency of the precipitating flux intensity with the solar EUV intensity. Such dependency is presently difficult to reconstruct with MAVEN coverage (from solar mean to solar minimum conditions) but should be reachable with MAVEN's second Mars year of operation. However, we can tentatively infer what could be such dependency from Dong et al. (2017) who reported an almost linear dependency of the low-energy tailward escaping ion flux with EUV intensity. Using such dependency for the heavy ion precipitation would imply a relatively modest cumulative total loss of atmosphere via sputtering during the last 4 Gyr (tens of mbar of CO_2 and less than 1 m of H_2O equivalent depth of an ocean covering the whole Martian surface) with respect to the expected quantity of atmosphere that should have escaped during that period. This extrapolation of sputtering-induced atmospheric escape loss following a linear dependency with EUV flux is however in contradiction with model (Chaufray et al., 2007) and will need further investigations of MAVEN data to be confirmed or contradicted.

Acknowledgments

This work was supported by CNES "Système Solaire" program and by the Programme National de Planétologie and Programme National Soleil-Terre. This work is also part of HELIOSARES Project supported by the ANR (ANR-09-BLAN-0223) and MARMITE project (ANR-13-BS05-0012-02). Authors also acknowledge the support of the IPLS data center CICLAD for providing us access to their computing resources and data. The results of the simulations presented in this paper are available at http://heliosares.latmos.ipsl.fr/EGM_Library.html.

References

- Bhardwaj, A., Thampi, S. V., Das, T. P., Dhanya, M. B., Naik, N., Vajja, D. P., et al. (2017). Observation of suprathermal argon in the exosphere of Mars. *Geophysical Research Letters*, *44*, 2088–2095. <https://doi.org/10.1002/2016GL072001>
- Chaufray, J.-Y., Gonzalez-Galindo, F., Forget, F., Lopez-Valverde, M., Leblanc, F., Modolo, R., et al. (2014). Three-dimensional Martian ionosphere model: II. Effect of transport processes due to pressure gradients. *Journal of Geophysical Research: Planets*, *119*, 1614–1636. <https://doi.org/10.1002/2013JE004551>
- Chaufray, J. Y., Modolo, R., Leblanc, F., Chantreau, G., Johnson, R. E., & Luhmann, J. G. (2007). Mars solar wind interaction: Formation of the Martian corona and atmospheric loss to space. *Journal of Geophysical Research*, *112*, E09009. <https://doi.org/10.1029/2007JE002915>
- Dong, Y., Fang, X., Brain, D. A., McFadden, J. P., Halekas, J. S., Connerney, J. E. P., et al. (2017). Seasonal variability of Martian ion escape through the plume and tail from MAVEN observations. *Journal of Geophysical Research: Space Physics*, *122*, 4009–4022. <https://doi.org/10.1002/2016JA023517>
- England, S. L., Liu, G., Yiğit, E., Mahaffy, P. R., Elrod, M., Benna, M., et al. (2017). MAVEN NGIMS observations of atmospheric gravity waves in the Martian thermosphere. *Journal of Geophysical Research: Space Physics*, *122*, 2310–2335. <https://doi.org/10.1002/2016JA023475>
- Fang, X., Bougher, S. W., Johnson, R. E., Luhmann, J. G., Ma, Y., Wang, Y.-C., & Liemohn, M. W. (2013). The importance of pickup oxygen ion precipitation to the Mars upper atmosphere under extreme solar wind conditions. *Geophysical Research Letters*, *40*, 1922–1927. <https://doi.org/10.1002/grl.50415>
- Fox, J. L. (2004). CO_2^+ dissociative recombination: A source of thermal and non-thermal C on Mars. *Journal of Geophysical Research*, *109*, A08306. <https://doi.org/10.1029/2004JA010514>
- Fox, J. L., & Bakalian, F. M. (2001). Photochemical escape of atomic carbon from Mars. *Journal of Geophysical Research*, *106*(A12), 28,785–28,795. <https://doi.org/10.1029/2001JA000108>
- Fox, J. L., & Hač, A. (1997). The $^{15}N/^{14}N$ isotope fractionation in dissociative recombination of N_2^+ . *Journal of Geophysical Research*, *102*(E4), 9191–9204. <https://doi.org/10.1029/97JE00086>
- Fox, J. L., & Hač, A. B. (2014). The escape of O from Mars: Sensitivity to the elastic cross sections. *Icarus*, *228*, 375–385. <https://doi.org/10.1016/j.icarus.2013.10.014>
- Gröller, H., Lichtenegger, H., Lammer, H., & Shematovich, V. I. (2014). Hot oxygen and carbon escape from the Martian atmosphere. *Planetary and Space Science*, *98*, 93–105. <https://doi.org/10.1016/j.pss.2014.01.007>
- Halekas, J. S., Taylor, E. R., Dalton, G., Johnson, G., Curtis, D. W., McFadden, J. P., et al. (2015). The Solar Wind Ion Analyzer for MAVEN. *Space Science Reviews*, *195*(1–4), 125–151. <https://doi.org/10.1007/s11214-013-0029-z>
- Hara, T., Luhmann, J. G., Leblanc, F., Curry, S. M., Halekas, J. S., Seki, K., et al. (2018). Evidence for crustal magnetic field control of ions precipitating into the upper atmosphere of Mars. *Journal of Geophysical Research: Space Physics*, *123*. <https://doi.org/10.1029/2017JA024798>

- Hara, T., Luhmann, J. G., Leblanc, F., Curry, S. M., Seki, K., Brain, D. A., et al. (2017). MAVEN observations on a hemispheric asymmetry of precipitating ions toward the Martian upper atmosphere according to the upstream solar wind electric field. *Journal of Geophysical Research: Space Physics*, *122*, 1083–1101. <https://doi.org/10.1002/2016JA023348>
- Jakosky, B. M., Lin, R. P., Grebowksy, J. M., Luhmann, J. G., Mitchell, D. F., Beutelschies, G., et al. (2015). The Mars Atmosphere and Volatile Evolution (MAVEN) mission. *Space Science Reviews*, *195*, 3–48. <https://doi.org/10.1007/s11214-015-0139-x>
- Jakosky, B. M., Slipski, M., Benna, M., Mahaffy, P., Elrod, M., Yelle, R., et al. (2017). Mars' atmospheric history derived from upper-atmosphere measurements of $^{38}\text{Ar}/^{36}\text{Ar}$. *Science*, *355*, 1408–1410. <https://doi.org/10.1126/science.aai7721a>
- Johnson, R. E., Schnellenberger, D., & Wong, M. C. (2000). The sputtering of an oxygen thermosphere by energetic O^+ . *Journal of Geophysical Research*, *105*(E1), 1659–1670. <https://doi.org/10.1029/1999JE001058>
- Leblanc, F., & Johnson, R. E. (2002). Role of molecules in pick-up ion sputtering of the Martian atmosphere. *Journal of Geophysical Research*, *107*(E2), 5010. <https://doi.org/10.1029/2000JE001473>
- Leblanc, F., Chaufray, J. Y., Modolo, R., Leclercq, L., Curry, S., Luhmann, J., & Jakosky, B. (2017). On the origins of Mars' exospheric nonthermal oxygen component as observed by MAVEN and modeled by HELIOSARES. *Journal of Geophysical Research: Planets*, *122*, 2401–2428. <https://doi.org/10.1002/2017JE005336>
- Leblanc, F., Modolo, R., Curry, S., Luhmann, J., Lillis, R., Chaufray, J. Y., et al. (2015). Mars heavy ion precipitating flux as measured by Mars Atmosphere and Volatile Evolution. *Geophysical Research Letters*, *42*, 9135–9141. <https://doi.org/10.1002/2015GL066170>
- Lee, Y., Combi, M. R., Tenishev, V., Bougher, S. W., & Lillis, R. J. (2015). Hot oxygen corona at Mars and the photochemical escape of oxygen: Improved description of the thermosphere, ionosphere, and exosphere. *Journal of Geophysical Research: Planets*, *120*, 1880–1892. <https://doi.org/10.1002/2015JE004890>
- Lewkow, N. R., & Kharhenko, V. (2014). Precipitation of energetic neutral atoms and induced non-thermal escape fluxes from the Martian atmosphere. *The Astrophysical Journal*, *790*(2), 98. <https://doi.org/10.1088/0004-637X/790/2/98>
- Lillis, R. J., Brain, D. A., Bougher, S. W., Leblanc, F., Luhmann, J. G., Grebowsky, J., et al. (2015). Characterizing atmospheric escape from Mars with MAVEN. *Space Science Reviews*, *195*(1–4), 357–422. <https://doi.org/10.1007/s11214-015-0165-8>
- Luhmann, J. G., & Kozyra, J. U. (1991). Dayside pickup oxygen ion precipitation at Venus and Mars: Spatial distributions energy deposition and consequences. *Journal of Geophysical Research*, *96*(A4), 5457–5467. <https://doi.org/10.1029/90JA01753>
- McFadden, J., Kortmann, O., Dalton, G., Abiad, R., Curtis, D., Sterling, R., et al. (2015). The MAVEN Suprathermal and Thermal Ion Composition (STATIC) instrument. *Space Science Reviews*, *195*(1–4), 199–256. <https://doi.org/10.1007/s11214-015-0175-6>
- Wang, Y.-C., Luhmann, J. G., Fang, X., Leblanc, F., Johnson, R. E., Ma, Y., & Ip, W.-H. (2015). Statistical studies on Mars atmospheric sputtering by precipitating pickup O^+ : Preparation for the MAVEN mission. *Journal of Geophysical Research: Planets*, *120*, 34–50. <https://doi.org/10.1002/2014JE004660>
- Yagi, M., Leblanc, F., Chaufray, J. Y., Gonzalez-Galindo, F., Hess, S., & Modolo, R. (2012). Mars exospheric thermal and non-thermal components: Seasonal and local variations. *Icarus*, *221*(2), 682–693. <https://doi.org/10.1016/j.icarus.2012.07.022>